RSC Advances

PAPER

View Article Online
View Journal | View Issue

Cite this: *RSC Adv.*, 2026, **16**, 3458

Medicinal chemistry meets nanotechnology: machine learning assisted colorimetric sensing platform for oxalic acid based on drug mediated copper oxide nanoparticles

Muhammad Ishtiaq Jan, *[a] Abda Khatoon,[a] Wei Sun,[b] Naeem Khan,[a] Sajid Ali,[c] Ibrahim A. Shaaban,[d] Mansoor Khan,[a] Amir Badshah,[a] Imran Rabbani[e] and Umar Nishan *[a]

Increased levels of oxalic acid are associated with an increased risk of kidney stone formation, which can lead to renal failure. In addition, its high concentration in the blood can lead to cardiovascular diseases. Therefore, it is vital to detect and quantify oxalic acid economically and rapidly. Copper oxide nanoparticles (CuONPs) are gaining importance as colorimetric nanosensors due to their intrinsic color change, cost-effectiveness, and easy synthesis. Paracetamol-mediated CuO NPs were synthesized through a new approach and characterized through various spectroscopic and morphological techniques. UV-visible spectroscopy confirmed the synthesis of CuO NPs through surface plasmon resonance at 225 nm. The peak at 850 cm^{-1} corresponds to the stretching vibration of CuO NPs. The XRD and SEM characterization techniques confirmed the particle size of 27.51 nm with a spherical morphology. A machine learning-assisted strategy was developed with four prediction models: Random Forest, Linear Regression, XGBoost, and Decision Tree Regression. The intrinsic colorimetric features of CuO NPs were observed through the naked eye and quantified through spectroscopy with the addition of oxalate. The developed platform selectively detected oxalate levels in concentrations ranging from 1 to 120 μM, with a limit of detection (LOD) of 0.23 μM and a limit of quantification (LOQ) of 0.78 μM. The developed biosensor successfully quantified oxalate, crucial for diagnosing hyperoxaluria and preventing calcium oxalate stone formation in the kidneys. The machine learning complementary tools further bolster the accuracy of colorimetric concentration prediction.

Received 17th November 2025
Accepted 4th January 2026

DOI: 10.1039/d5ra08862c

rsc.li/rsc-advances

1. Introduction

The most significant sources of oxalic acid are plants, and it is critical to various biological systems.[1] However, due to its acidic nature, the potential of oxalic acid to form metallic complexes is very high, and this condition provides substantial support for the formation of kidney stones.[2] Generally, small quantities of oxalic acid are produced within the body through the metabolism of some amino acids, vitamins, and minerals, which are usually excreted through the urine at a rate of 10 to 50 mg/day[3]. Hyperoxaluria affects many more serious conditions other than the mere development of kidney stones; it leads to the dysregulation of minerals and also cardiovascular complications, even affecting neurological disorders.[4] The process initiated by hyperoxaluria promotes renal cell apoptosis directly during the formation of stones.[5] Hence, hyperoxaluria is a grave health risk around the world and requires effective treatment methods after proper diagnosis.[6] The medicinal industry greatly relies on oxalic acid as an excipient during the formulation of drugs. The food industry also applies oxalic acid as a preservative and in the purification of food material.[7] However, due to its ability to scavenge free radicals, oxalic acid can be effectively incorporated into formulations for skin care lesions, thereby preventing oxidative damage to cells.[8]

The sensing of oxalic acid has previously been reported through electrochemical,[9] spectroscopic chromatographic[10,11] and enzymatic methods.[12] These mentioned techniques, despite their merits, suffer from factors like high cost, difficult

[a]*Department of Chemistry, Kohat University of Science and Technology, Kohat 26000, Khyber Pakhtunkhwa, Pakistan. E-mail: umarnishan85@gmail.com; mishtiaqjan@kust.edu.pk*

[b]*Hainan International Joint Research Center of Marine Advanced Photoelectric Functional Materials, College of Chemistry and Chemical Engineering, Hainan Normal University, Haikou 571158, P. R. China*

[c]*Department of Chemistry, Bacha Khan University, Charsadda 24420, Khyber Pakhtunkhwa, Pakistan*

[d]*Central Labs, King Khalid University, P.O. Box 960, AlQura'a, Abha, 61413, Saudi Arabia*

[e]*Department of Pharmacy, Kohat University of Science and Technology, Kohat 26000, Khyber Pakhtunkhwa, Pakistan*

operation and maintenance, and sample pretreatment. On the other hand, the colorimetric sensing approach can offer a more viable alternative in terms of much lower cost, easy operation, and portability and does not require personnel with special skills.[13,14] The rise of nanotechnology has resulted in a renewed interest in the field of colorimetric nanosensors.

Preceding nanomaterials, various sensing platforms were reported based on natural enzymes such as horseradish peroxidase and glucose oxidase, *etc.* However, natural enzymes suffer from various shortcomings, such as lower stability, difficult handling, high cost, and low shelf life.[15] Various nanomaterials, such as manganese dioxide (MnO_2) nanosheets,[16] silver (Ag) NPs have been explored for the determination of oxalic acid.[17] The strong surface plasmon resonance, distance-dependent optical properties, and the ability to generate visually detectable signals make nanomaterials excellent candidates for colorimetric sensing applications. Specifically, the copper ion complex acts as a sensor, which indicates the presence of oxalate through a distinct color change upon selective binding.[18] This innovative system uses a pyrrole-containing copper complex and chromeazurol S to visually detect oxalate, changing color from blue to yellow upon addition of oxalate. However, the use of chromeazurol S dye is associated with skin and eye irritation.[19] The literature study revealed that oxalic acid was quantified with an electrochemical Ag-NPs and nitrogen-doped graphene oxide (N-GO) nanocomposite. The exceptional performance of the sensor, including its current response, excellent selectivity, and high stability, is attributed to the beneficial synergistic interaction between the Ag-NPs and N-GO.[9] An electrochemical sensor for oxalic acid detection was developed using palladium nanoparticle-loaded carbon nanofiber (Pd/CNF) composites. The well-dispersed Pd nanoparticles on the carbon nanofibers gave the sensor high electrocatalytic performance and rapid voltametric responses with a complex procedure.[20] However, high-cost metal nanoparticle-based systems that use expensive elements like Au, Pt, or Pd are not desirable because they elevate the cost of testing. In addition, different nanoparticles have been developed for the colorimetric sensing of oxalic acid due to several advantages, including low cost, rapidity, and being easy availability.[17,21–24]

The safety record of paracetamol in clinical settings makes it a promising candidate for biomedical applications of nanoparticle synthesis.[25] Its rich electron density can help in the reduction of the metal salt in the synthesis of the nanoparticles. The paracetamol drug stabilizes nanoparticles, mitigating nanoparticle agglomeration and enhancing colloidal stability in diverse media, including biological fluids. Additionally, its antioxidant activity synergizes with the intrinsic properties of nanoparticles such as CuO NPs, potentially providing a dual therapeutic advantage in addressing oxidative stress-related pathologies.

The novelty of this work lies in the synthesis and use of paracetamol-mediated CuO NPs for the colorimetric sensing of oxalic acid. Comprehensive characterization of the synthesized nanoparticles and their functionalization was performed. The synthesized platform was successfully used for the detection and quantification of oxalic acid with excellent precision, sensitivity, and selectivity. It was also applied for the detection and quantification of oxalic acid in urine samples. The method further advances innovation by coupling these tailored nanoparticles with machine-learning algorithms to optimize colorimetric response patterns, enabling precise quantification, improved limit of detection, robust prediction accuracy, and accurate prediction of oxalic acid concentrations with improved sensitivity and precision. The data-driven computational layer transforms the sensor from a qualitative color-change system into a robust quantitative analytical tool.

2. Materials and methods

2.1 Reagents

CuO NPs were synthesized using paracetamol, copper(II) sulfate pentahydrate ($CuSO_4.5H_2O$), dimethyl sulfoxide (DMSO), acetic acid, and sodium hydroxide (NaOH). The oxalic acid was used as an analyte. The reagents were of analytical grade and used as received from Sigma-Aldrich, USA. All the solutions were prepared using deionized water.

2.2 Synthesis of CuO NPs

CuO NPs were synthesized using 500 mg of paracetamol dissolved in DMSO. The resulting solution was magnetically stirred for 10 minutes at room temperature and filtered. The filtrate was then added dropwise to a 50 mM copper(II) sulfate solution and magnetically stirred for 4 hours. The resulting solution was centrifuged at 1100 rpm for 20 minutes to isolate the CuO NPs as a pellet. The obtained CuO NPs were subsequently dried at 50 °C and stored at room temperature for further analysis.[26]

2.3 Instrumentation

The characteristic peak for the synthesis of CuO NPs was investigated by UV-vis spectroscopy. The functional groups of synthesized CuO NPs were identified by Fourier transform infrared spectroscopy (FTIR) using an MX-300 spectrometer, with characteristic stretching vibrations at characteristic peaks.[27] The scanning electron microscopy (SEM) (JSM-5910) was used for studying the surface morphology of synthesized CuO NPs. High-resolution images of the nanoparticles were taken to examine the shape and morphology.[28] The X-ray diffraction (XRD) (Bruker Smart Apex) was used to investigate the crystalline nature of the developed CuO NPs. The particle size of NPs was calculated using the Debye–Scherrer equation.[29] The X-ray photoelectron spectroscopy (XPS) (EscaLab 250Xi Thermo, USA, with Al Kα X-ray radiation) analysis was used for the oxidation state and elemental composition of CuO NPs by measuring the binding energy of the released electrons.[30]

2.4 Functionalization of CuO NPs with acetic acid

The stability and prevention of agglomeration of CuO NPs were performed through functionalization with acetic acid. For this purpose, 6 mg of the NPs were taken in 1 mL of acetic acid for 30 minutes with continuous stirring till a homogeneous solution was obtained. The bluish dispersion of functionalized CuO NPs was stored for further study.[31]

2.5 Colorimetric sensing of oxalic acid

The colorimetric sensing of oxalate was investigated at ambient temperature and pH 7. The assay was performed with 100 μL of 10 μM oxalate solution mixed with 250 μL of CuO NPs in an Eppendorf tube. The blue color of the capped CuO NPs was rapidly transitioned to a colorless solution with the addition of oxalate. The assay response was readily observed by the naked eye, with a visual change, and subsequently confirmed using a UV-vis spectrophotometer. The real urine samples were collected from Kohat Development Hospital (KDA), Kohat, Khyber Pakhtunkhwa, Pakistan. The research work was approved by the ethical committee of Kohat University of Science and Technology, Kohat, Pakistan, under Reference No: Ref-No/KUST/Ethical Committee/528.

2.6 Machine learning analysis of RGB-concentration relationship

Colorimetric images of oxalic acid solutions were resized uniformly, and their red (R), blue (B), and green (G) values were determined by using the Python Imaging Library.[32] RGB values were then correlated with the known concentrations of oxalic acid solutions. To perform machine learning, four prediction models were selected: Random Forest, Linear Regression, XGBoost, and Decision Tree Regression.[33] These models were trained on a dataset that consisted of 01 blank and 16 samples of different concentrations (from 1 to 120 μM) of oxalic acid solutions along with their respective RGB values. The train-test technique was used to evaluate the performance of models. For this purpose, the data was divided into 80% training and 20% testing subsets. Performance of the models was evaluated using evaluation metrics such as Mean Absolute Error (MAE), Root Mean Square Error (RMSE), and the coefficient of determination (R^2).[34] The machine learning approach indicates its potential to combine with colorimetric analysis as a quick and portable supporting tool for concentration estimation of oxalic acid.

3. Results and discussion

3.1 Potential of the calorimetric method for sensing oxalic acid

The reaction of capped CuO NPs with acetic acid involves the coordination of oxalic acid with the Cu^{2+} ions on the surface of the CuO NPs, effectively converting the CuO into copper oxalate, CuC_2O_4. This leads to a change in the optical properties of the nanoparticle, which is demonstrated by a color change in the NP solution and hence forms a basis for a colorimetric assay. This is a reliable method for quantifying oxalic acid concentration in various samples, as illustrated in Scheme 1.

3.2 Characterization of CuO NPs

The characterizations of the synthesized CuO NPs were performed for optical, structural, size, and morphological properties. Moreover, the identification of surface functional groups is a necessity for a comprehensive understanding of their nature.

3.2.1 UV-vis spectroscopy. The reaction was carefully monitored for the optimal absorption characteristics, targeting the surface plasmon resonance. For this purpose, 300 μL of the capped copper oxide nanoparticles were mixed with 1 mL of water. The surface plasmon resonance peak at 225 nm validated the successful synthesis through UV-vis spectroscopy for further use in sensing applications of CuO NPs, as shown in Fig. 1. In addition, the synthesis of the biosensor was confirmed through UV-vis spectroscopy as reported earlier.[35–37]

3.2.2 FTIR spectroscopy analysis. The function groups of synthesized CuO NPs were identified with FTIR. The FTIR spectrum of the sample reveals a broad peak at 3390 cm^{-1} for O–H stretching, indicating the presence of hydroxyl groups due

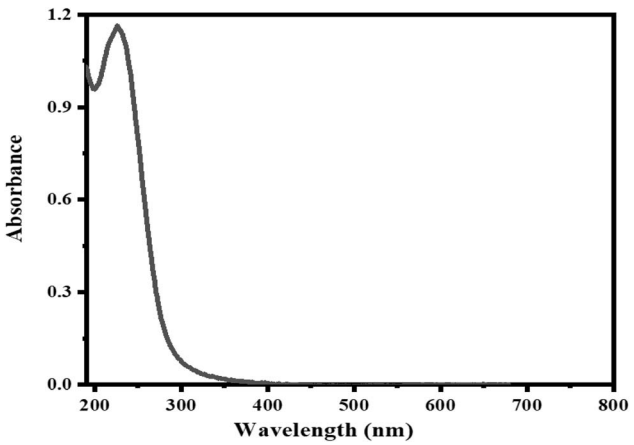

Fig. 1 The UV-vis absorption spectrum of the synthesized CuO NPs.

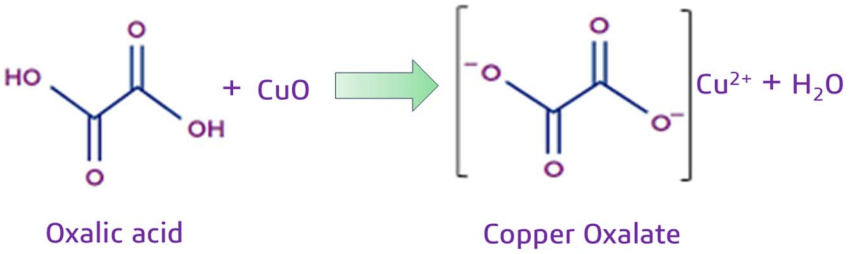

Scheme 1 Detection of oxalate with CuO NPs utilizing their intrinsic properties. The blue CuO NPs undergo a chemical reaction after incorporation of oxalic acid, forming copper oxalate. This reaction causes a striking blue-to-colorless transition, which can then be precisely used to measure the amount of oxalic acid present in various samples.

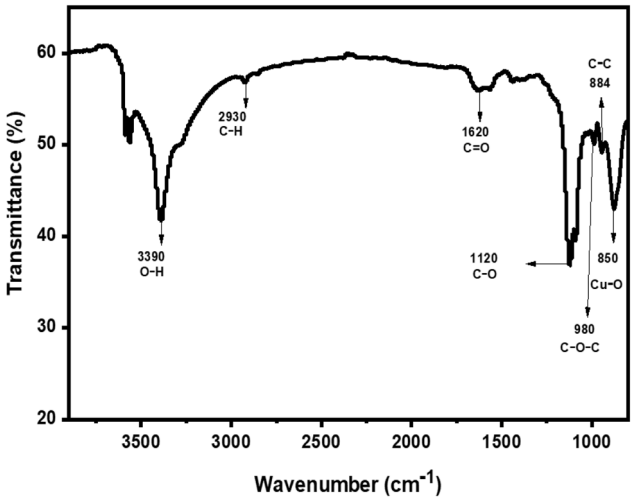

Fig. 2 FTIR spectrum of the synthesized CuO NPs with characteristic stretching vibration of respective functional groups.

to residual water or the drug used for the synthesis of CuO NPs. The C–H stretching is represented by the peak at 2930 cm^{-1}, which indicates the presence of alkyl groups. It originated from the organic components of the drug used. A peak at 1620 cm^{-1} represented C═O stretching, a characteristic feature of carbonyl groups and, precisely, carboxyl groups belonging to the drug. The peak at 1120 cm^{-1} corresponds to C–O stretching. It suggests the presence of esters, ethers, or alcohols. The peak at 980 cm^{-1} indicates C–O–C stretching. It shows the ether linkages within the drug structure. The peak at 884 cm-1 corresponds to the C–C stretching, which indicates the organic backbone of the drug. Lastly, the peak at 850 cm^{-1} has confirmed the presence of Cu–O stretching vibration and hence validates the synthesis of the CuO NPs[27,38] as shown in Fig. 2.

3.2.3 XRD analysis of CuO NPs. The XRD analysis provides crucial information on CuO NPs regarding crystal phase, crystallite size, lattice parameters, and the general crystallinity of the material.[39] The obtained XRD patterns showed the presence of pronounced crystallographic phases of CuO NPs. The sharp and well-defined peaks at specific 2θ values provide evidence for the crystallinity of the prepared CuO NPs. The peak with the highest intensity related to a plane of (111) can be considered as the preferential crystallographic orientation, as shown in Fig. 3. Furthermore, there are additional peaks at planes such as (101), (110), and (020), which reveal the polycrystalline nature of NPs, as verified by JCPDS card no. (05-0661). However, a sharp and well-defined peak manifests the high crystallinity of the drug-mediated CuO NPs.[40,41] The absence of extraneous peaks confirms the purity of the synthesized CuO NPs. The Debye–Scherer equation was used to calculate the average crystallite size to be 27.51 nm, a result consistent with expected values for CuO NPs.

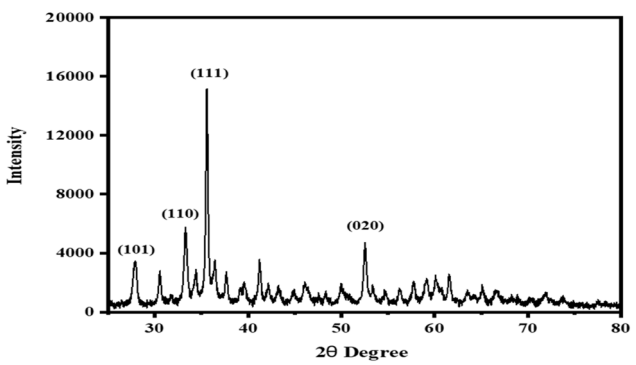

Fig. 3 XRD pattern of synthesized CuO NPs with different peaks.

3.2.4 XPS analysis. XPS was used to analyze the synthesized nanoparticles, providing information about elemental composition and surface oxidation states of the constituent elements. The survey spectrum and the deconvoluted spectra of the constituent elements of the synthesized nanoparticles are shown in Fig. 4. The XPS analysis revealed the binding energies of the respective elements present in CuO NPs.[42] The O 1s peak observed at 529.18 eV confirmed the presence of oxygen, consistent with previous findings in the literature.[43] The C 1s peak, observed at 284.8 eV, indicated the presence of carbon, likely originating from the drug coating. The deconvoluted spectrum of the Cu 2p revealed Cu 2p3/2 and Cu 2p1/2 peaks at 933.5 eV and 953.16 eV, respectively. This confirmed the +2 oxidation state of Cu in the CuO NPs. The presence of satellite peaks further supported this finding. The O 1s peak at 529.18 eV was characteristic of O^{-2} in CuO NPs, while a peak at 531.08 eV suggested the presence of other oxygen species, possibly hydroxyl groups (O–H) from the drug. The high-resolution C 1s peak at 284.8 eV, which is typically associated with C–C or C–H bonds, indicated the presence of organic material, likely originating from the drug.[44,45]

3.2.5 SEM and HRTEM analysis. SEM and high-resolution transmission electron microscopy (HRTEM) are key tools in nanomaterials analysis, providing high-resolution images that illuminate intricate surface features. Hence, the correct measurement of the shape, size, and morphology of nanoparticles through the application of these techniques is a vital factor that affects their properties and applications.[36] Fig. 5(A) and (C) shows SEM images at different magnifications. The images clearly indicate that the synthesized CuO NPs occur in spherical/quasi-spherical morphology. In addition, Fig. 5(D–F) provides further insight into the HRTEM images and corroborates the findings of the SEM analysis. The well-defined lattice fringes investigated through HRTEM revealed the high crystallinity of the synthesized CuO NPs.

3.3 Colorimetric sensing of the proposed reaction

The addition of 100 μL oxalic acid with a concentration of 10 μM was added to 250 μL acetic acid-capped CuO NPs with 50 mM concentration, resulting in a distinct colorimetric transition from blue to light blue, confirming the reaction. The response between capped CuO NPs and oxalic acid was further optimized with respect to various parameters to obtain a transparent solution. The visual change was observed with a decrease in the peak intensity at 225 nm through spectrophotometric analysis. The consistent and reproducible relationship between the

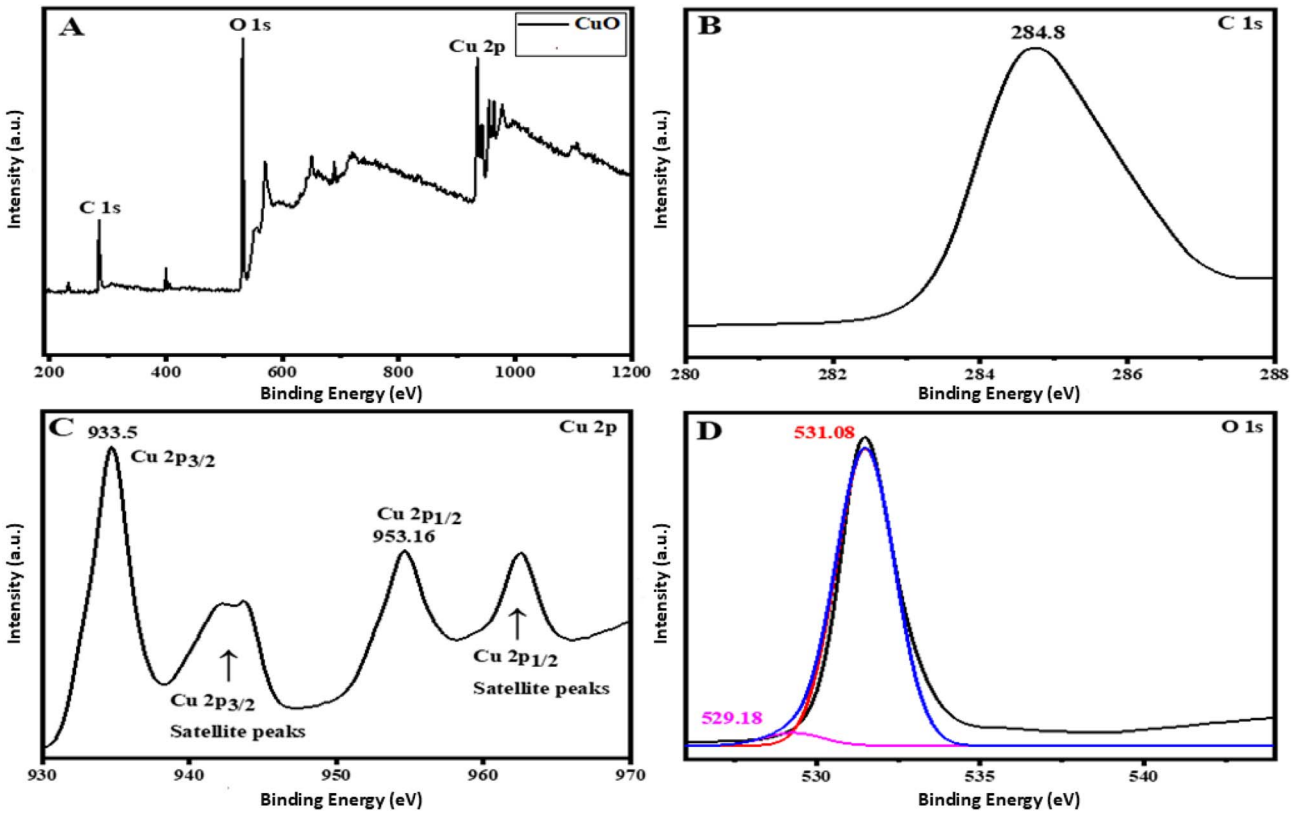

Fig. 4 XPS pattern of the synthesized CuO NPs showing the composition and surface chemical state of the elements present in the synthesized nanoparticles.

increasing oxalic acid concentration and the observed reduction in peak intensity at 225 nm provides strong validation for the use of acetic acid-capped CuO NPs as a colorimetric sensor for detecting oxalic acid, as shown in Fig. 6.

3.4 The optimization of various parameters for the colorimetric sensing of oxalic acid

Several factors affecting the performance of CuO NPs were optimized. This was done using a standard approach, where

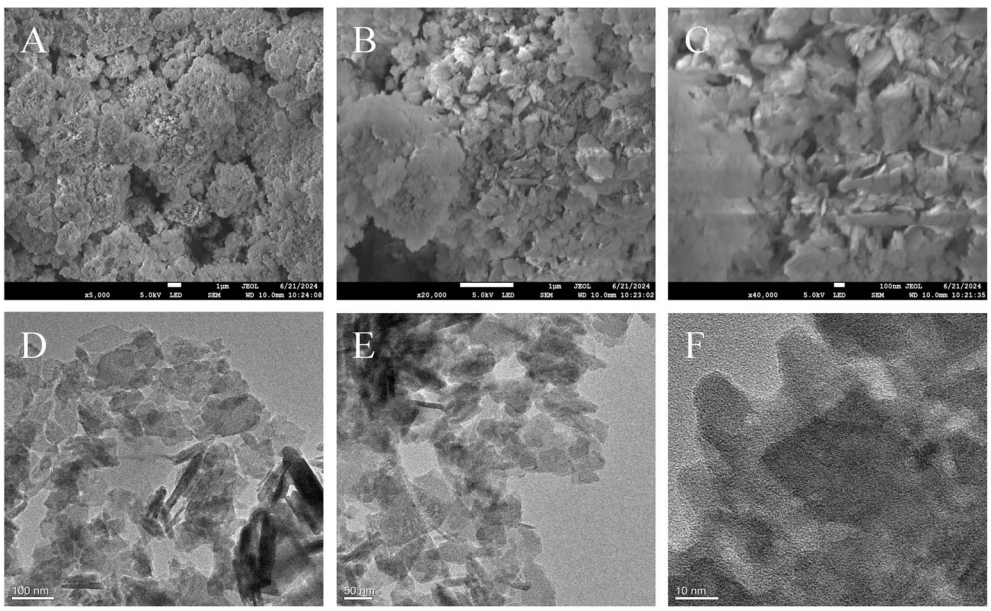

Fig. 5 Scanning electron microscopy images of the synthesized nanoparticles (A–C) and high-resolution transmission electron images showing their lattice fringes (D–F).

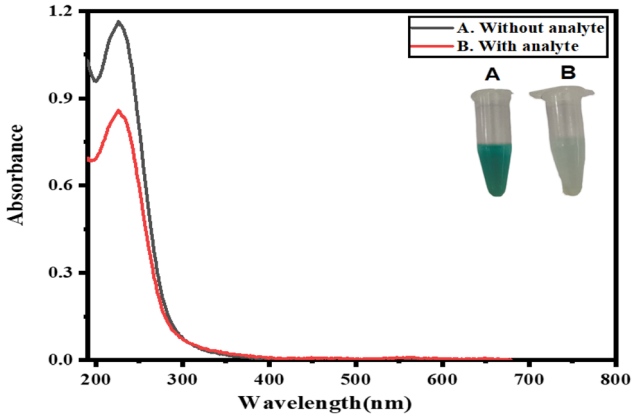

Fig. 6 UV-visible spectrum of CuO NPs. A: CuO NPs without the addition of oxalate solution have high absorbance. B: CuO NPs with the addition of oxalate have low absorbance.

one variable was changed while the others remained constant. However, all the different factors influencing the performance of the proposed sensor were successfully optimized.

3.4.1 Optimization of capped CuO NPs. The aggregation of colloidal nanoparticles in solution was overcome by chemically binding a protective agent to their surface, thus maintaining a stable dispersion and preserving their unique properties.[46] Therefore, in the present findings, CuO NPs were uniformly suspended in acetic acid and utilized as a colorimetric sensor for oxalic acid detection. The performance of the sensor was directly influenced by nanoparticle concentration. The colorimetric response of the nanoparticles to oxalic acid varied with nanoparticle concentration. However, effective detection was achieved only at an optimum concentration after observing the colorimetric response of capped CuO NPs in the range of 50 μL to 400 μL with the concentration of 50 mM. The lower concentrations of nanoparticles limited the binding of oxalic acid to their surface, therefore preventing a discernible color change. Furthermore, the binding of capped CuO NPs was increased and resulted in a distinct color change from blue to transparent upon the addition of 100 μL (10 μM) of oxalic acid to 250 μL of the capped nanoparticle solution. Hence, 250 μL of

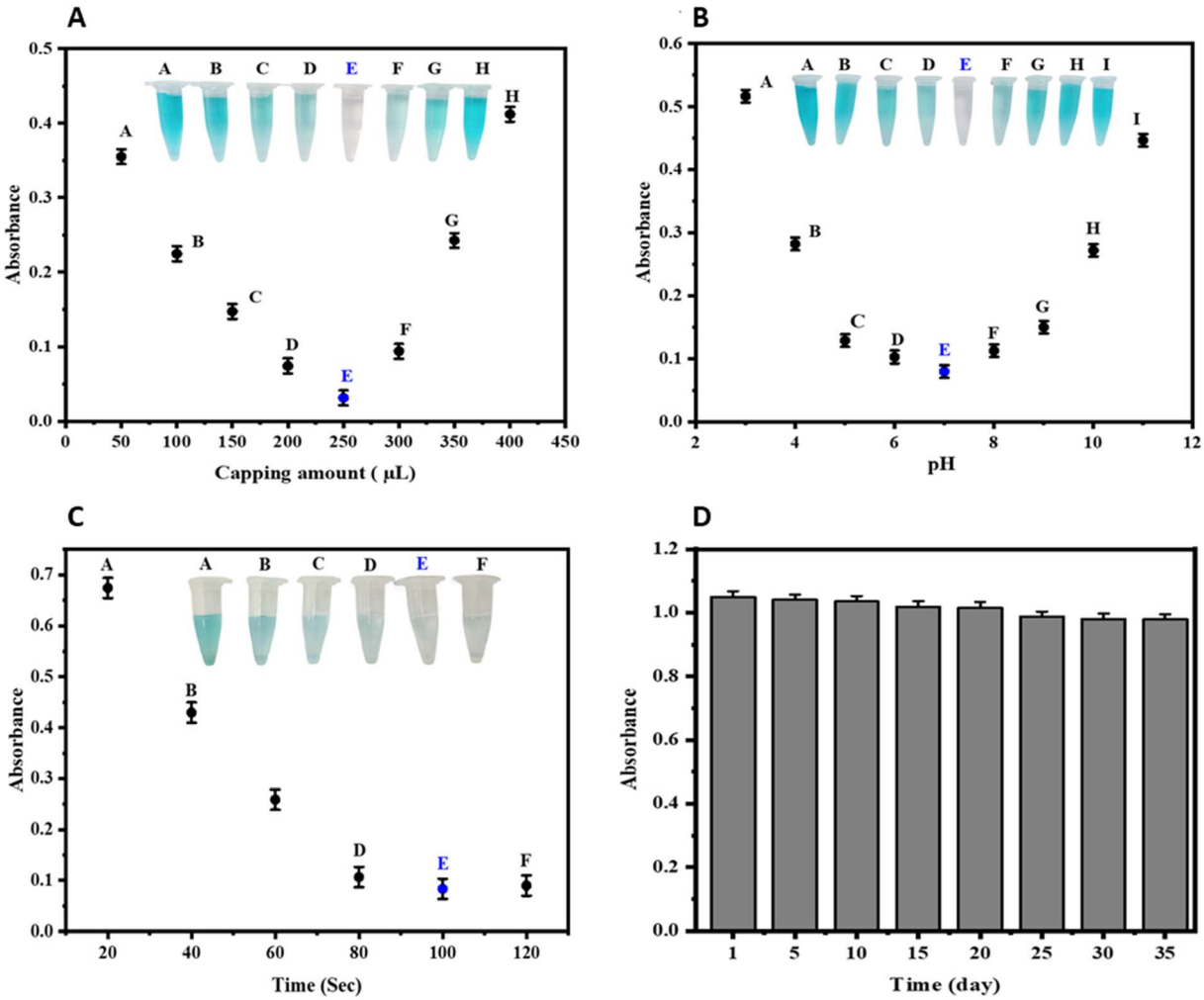

Fig. 7 The optimization of CuO NPs through different parameters for the sensing of oxalate. (A) The optimization for functionalization of CuO NPs with different concentrations of acetic acid. (B) The optimization of pH for the sensing activities of synthesized CuO NPs. (C) The time optimization for the sensing activities of CuO NPs. (D) Show the stability of the platform over a period of 35 days.

the capped nanoparticles was used as the optimum for onward reactions, as shown in Fig. 7(A).

3.4.2 Effect of pH. The pH range 3 to 12 was used to determine the optimum pH response of the proposed sensor using standard buffer solutions for accurate pH value adjustments.[47] The colorimetric sensitivity of the sensor was highly dependent on pH, which affects both the reaction kinetics of the capped CuO NPs with oxalic acid and the stability of the nanoparticles. Indeed, the sensor showed its best performance at neutral pH 7. However, below pH 7, the addition of oxalic acid led to a color change from bluish to transparent. The spectrophotometric analysis at 225 nm performed has confirmed that pH 7 is the optimum pH at which maximum colorimetric change can be achieved during the detection of oxalic acid, as illustrated in Fig. 7(B).

3.4.3 Effect of time and stability of biosensor. The reaction time influences the performance of the Cu NPs sensor, as illustrated in Fig. 7(C). The relationship between the time that CuO NPs were exposed to the oxalate and their resulting reactivity determined the optimal reaction time. The results showed a clear peak in sensor activity at 100 seconds. Therefore, the optimal reaction time for the colorimetric detection of oxalic acid was determined to be 100 seconds. This is significantly better when compared to previously reported methods requiring up to a 30-minute reaction time.[48,49] Therefore, the developed sensor offers a substantially faster detection capability for oxalic acid when compared to the literature. Thus, the fast response time of the present sensor underlines the potential of the sensor for analysis in efficient and rapid analysis in various applications. The stability study was conducted over a period of 35 days, and the nanoparticles were found to be stable, and there was no significant variation in their efficacy, as shown in Fig. 7(D).

3.5 The analytical characteristics of the fabricated CuO NPs biosensor

The analytical performance of the fabricated sensor for oxalic acid detection was evaluated, and the corresponding spectroscopic data are presented in Fig. 8(A). The incremental addition of oxalic acid led to a discernible colorimetric transition from blue to colorless, accompanied by a concomitant decrease in the spectroscopic absorption peak intensity at 225 nm. The systematic investigation was conducted across a concentration range of oxalic acid spanning 1 to 120 μM, revealing a direct interaction between the analyte concentration and the optical response of the fabricated sensor. Moreover, the developed sensor accurately detected oxalic acid concentration within the LOD of 0.23 μM and LOQ of 0.78 μM, as shown in Fig. 8(B). The

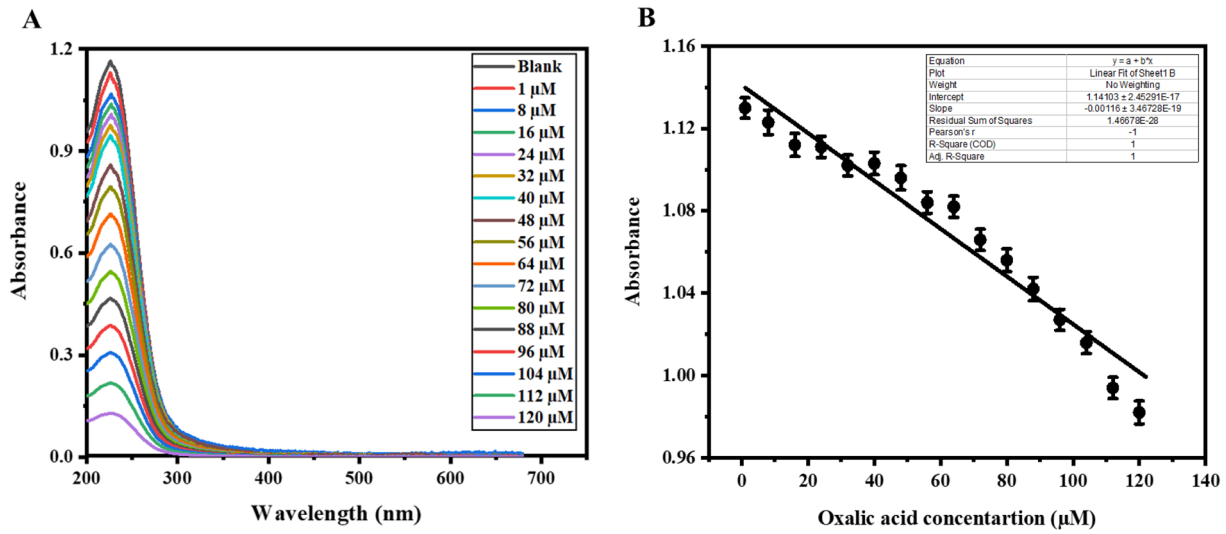

Fig. 8 (A) The decreasing intrinsic property of CuO NPs with increasing concentration of oxalic acid solution. (B) The collaboration graph of various concentrations of oxalic acid solution using CuO NPs.

Table 1 Comparison of the proposed sensor with already reported colorimetric sensors for the detection of oxalic acid

Sr #	Material used	Method	Linear range (μM)	LOD (μM)	References
1	CURNs	Colorimetry	1.6–18.8	0.77	21
2	AgNPs	Colorimetry	10–40	3.3	22
3	c-MWCNT/Au GNPs	Colorimetry	1–800	1	51
4	FeSSA	Colorimetry	4.5–888	4	23
5	PtNPGNs	Colorimetry	100–50000	5	52
6	Ag-Nps + N-GO	Colorimetry	10–300	2	9
7	CuO NPs@CH_3COOH	Colorimetry	1–120	0.23	Present work

oxalic acid was also colorimetrically quantified with curcumin-mediated nanoparticles in the presence of Fe(III). The method was complex and based on the inhibitory effect of oxalate ion on the reaction with Fe(III) in acidic media within a linear range of 0.15 to 1.70 μM[21]. Moreover, oxalic acid is predominantly present in natural products, and different approaches were used to quantify its concentration and cope with its drastic effects.[22] The oxalic acid was also determined using oxalate oxidase and sensors based on the injection of the recognition element technology, with a linear range of 0 and 5 mM.[50] The amperometry biosensor with a complex approach was prepared using a multi-walled carbon nanotube-gold nanoparticle composite for oxalate determination. The electrocatalytic response revealed a linear range of oxalic acid concentrations from 1 to 800 μM, with a good detection limit of 1 μM. However, the utilization of gold nanoparticles increased the sensor's cost.[51] The present proposed sensor was compared with previously reported literature, as shown in Table 1. The proposed developed sensor demonstrated robust quantitative capabilities for oxalic acid determination. Notably, the sensor exhibited rapid kinetic behavior, achieving a response time within 100 seconds. Therefore, the analytical merits obtained from the present study have several advantages over previously reported sensor systems for oxalic acid detection in the context of cost-effectiveness, easy approach synthesis, and rapid response with lower LOQ.

3.6 Interference study

The interference study of the developed biosensor was performed with various metal ions, including calcium and magnesium. In addition, different biomolecules, including glucose, lysine, trypsin, and uric acid. The selectivity of the present sensor was also investigated in structurally similar compounds, including oxalic acid, pyruvic acid, maleic acid, and glutamic acid, to assess potential interference. Moreover, an equal concentration (100 μM) of the other tested species did not elicit a similar response or interfere with detection under the experimental conditions optimized for oxalic acid. The developed sensor exhibited a significant colorimetric response only for oxalic acid and observed a notable decrease in absorbance at 225 nm. Therefore, the high sensitivity of CuO NPs toward oxalic acid makes them excellent colorimetric probes. Thus, the sensor is highly selective toward the detection of oxalic acid, which promises the applicability of the sensor for selective detection, as schematically shown in Fig. 9.

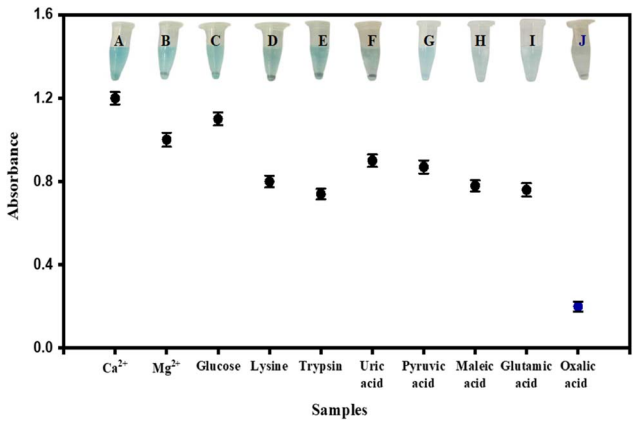

Fig. 9 The selectivity of CuO NPs for the sensing of oxalic acid in the presence of various potential interfering species.

3.7 Real sample analysis of urine

The high percent recovery of oxalic acid from the real urine sample using the CuO NPs sensor confirms its accuracy and efficiency for oxalic acid detection. Within the complex biological matrix, the detection of oxalic acid indicates minimal interference and reliable quantification under optimal conditions. The CuO NPs colorimetric sensor was used to directly measure the oxalate ions in real samples, as shown in Fig. 10. The proposed sensor was validated by assessing the recovery of spiked oxalate solutions at concentrations of 0.7, 2, 3.5, 11.5, and 16 μM, given in Table 2. The results were calculated using the percentage recovery formula and are summarized as follows:

$$\text{Recovery\%} = \text{oxalate found/oxalate added} \times 100.^{18}$$

3.8 Predictive modeling of concentration from RGB values

The performance of predictive machine learning models was evaluated by comparison of predicted values of oxalic acid concentrations with actual concentrations, as shown in

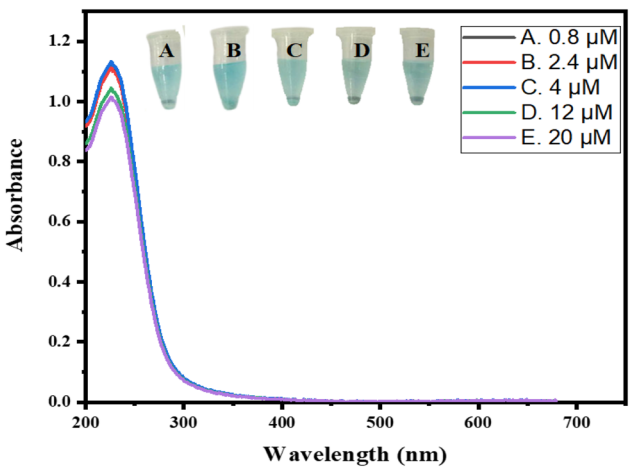

Fig. 10 The detection of various concentrations of oxalic acid in real urine samples.

Table 2 The detection of oxalate levels in real samples

Samples	Spike level (μM)	Spike added (μM)	Found (μM)	Spike recoveries (%)	RSD (%)
1	0.1	0.7	0.8	114.28	1.25
2	0.4	2	2.2	110	4.54
3	0.5	3.5	3.9	111.428	2.56
4	0.51	11.5	12.4	107.88	2.41
5	2.23	16	18.1	113.12	1.1

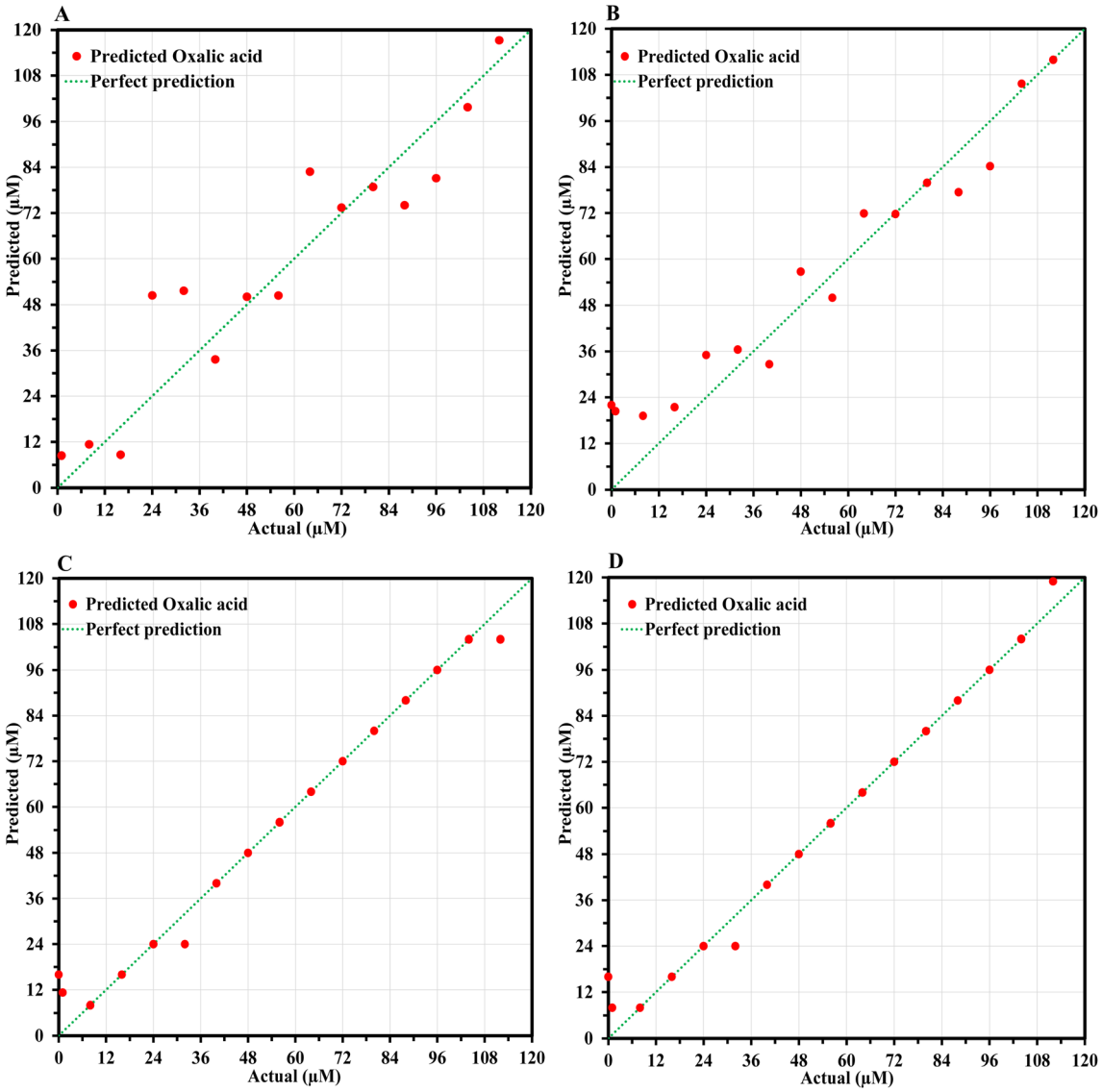

Fig. 11 Actual values of oxalic acid dilutions against predicted values obtained by ML models (A) linear regression, (B) Random Forest, (C) XGBoost Regression, (D) Decision Tree.

Fig. 11(A–D). Decision tree (DT) and XGBoost (XGB) regressors have shown apparently the best performance due to slightly lower RMSE and MAE and higher R^2 (Table 3 and Fig. 12). However, the overall predicted results of these two models revealed overfitting of models due to the limited dataset. In contrast, Random Forest (RF) and Linear Regression (LR) models performed well by producing more stable and chemically interpretable results. The RF model handled the non-linear relationship in the data without becoming too complex, while the simpler model, LR, revealed a steady trend between actual and predicted concentrations. Overall, both models have given consistent predictions of all concentrations of oxalic acid. Although XGB and DT mathematically overtook other models, in the context of colorimetric analysis, where reproducibility and interpretation are critical, RF and LR were chosen as reliable models regardless of little higher error values. The relationship between RGB values and oxalic acid concentrations demonstrated a clear trend, as shown in Fig. 13. These results indicate that simpler models like random forest and linear regression can perform well compared to complex models, especially when the data set is small and linearity is evident. The performance gap observed for XGB and DT may be attributed to insufficient data points for these algorithms to

Table 3 Mean Absolute Error (MAE), Root Mean Square Error (RMSE), and the coefficient of determination (R^2) of all the ML models

Model	MAE	RMSE	R^2
Linear regression	14.629	16.993	0.861
XGBoost regression	10.571	11.065	0.941
Random forest	11.490	14.836	0.894
Decision tree regression	9.750	10.404	0.948

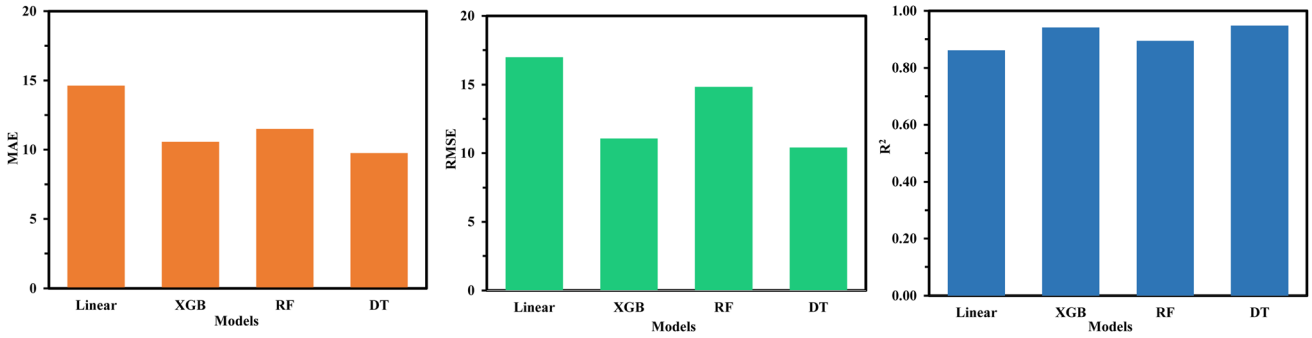

Fig. 12 Metrics comparison of all the ML models.

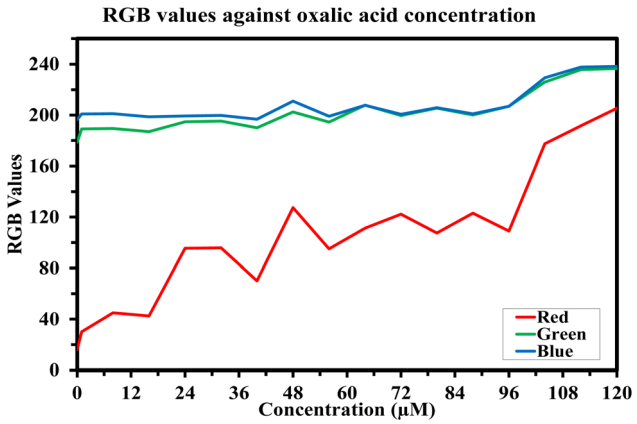

Fig. 13 RGB values for different concentrations of oxalic acid.

generalize effectively. These results specify that machine learning can be a complementary and supportive tool to colorimetric methods for concentration prediction.

4. Conclusions

The present research work demonstrates a successful, facile, and cost-effective drug-mediated synthesis of CuO NPs through a drug-mediated approach. All the spectroscopic and morphological analyses confirmed their synthesis. The surface functionalization, deagglomeration, and conductivity enhancement of the synthesized nanoparticles were successfully achieved through their capping with acetic acid. The acetic acid-capped CuO NPs revealed a colorimetric response to oxalic acid at a surface plasmon resonance of 220 nm, unequivocally establishing their potential as a colorimetric sensor. The readily observable color change from blue to transparent resulted from the interaction between CuO NPs and oxalic acid and was observed at 250 μL of capped nanoparticles, 100 μL of oxalic acid (10 μM), and pH 7, with a reaction time of 100 seconds at room temperature. The fabricated colorimetric CuO NPs sensor selectively detected oxalic acid with an LOQ of 0.78 μM. The research findings unveil a promising pathway for the development of rapid, on-site oxalic acid detection that can potentially be used for diverse applications. In addition, these findings confirmed the machine learning capability as a swift, portable enhancement to colorimetric methods for accurate oxalic acid concentration quantification.

Author contributions

Muhammad Ishtiaq Jan: writing – original draft, methodology, investigation, formal analysis, conceptualization, supervision. Abda Khatoon: writing – review & editing, investigation, formal analysis. Wei Sun: writing – review & editing, data curation, formal analysis. Naeem Khan: writing – review & editing, formal analysis, conceptualization. Sajid Ali: writing – review & editing, methodology, formal analysis. Ibrahim A. Shaaban: writing – review & editing, validation, funding acquisition. Mansoor Khan: writing – review & editing, methodology, formal analysis. Amir Badshah: writing – review & editing, data curation, formal analysis. Imran Rabbani: writing – review & editing, formal analysis, methodology. Umar Nishan: writing – review & editing, methodology, formal analysis, conceptualization, supervision.

Conflicts of interest

The authors declare no conflict of interest.

Data availability

All relevant data are presented within the manuscript; however, additional information is available upon request to the corresponding author based on reasonable demand.

Acknowledgements

The authors would like to extend their appreciation to University Higher Education Fund for funding this research work under Research Support Program for Central labs at King Khalid University through the project number CL/PRI/C/16.

References

1 M. U. Hasan, Z. Singh, H. M. S. Shah, J. Kaur, A. Woodward, E. Afrifa-Yamoah and A. U. Malik, *Postharvest Biol. Technol.*, 2023, **206**, 112574.
2 S. Milardović, Z. Grabarić and B. S. Grabarić, *Food Technol. Biotechnol.*, 2000, **38**, 203–210.

3 B. Beck, P. Cochat and Y. Frishberg, in *Pediatric Nephrology*, 8th edn, 2022, pp. 831–846.
4 N. Stepanova, V. Driianska, L. Korol, L. Snisar and L. Lebed, *Korean J. Intern. Med.*, 2022, **37**, 167–178.
5 L. Li, Y. Peng, M. Liu, Z. Wang, Q. Wang, S. Ming, X. Gao and Y. Sun, *Discov. Med.*, 2019, **28**, 75–85.
6 L. Frassetto and I. Kohlstadt, *Am. Fam. Physician*, 2011, **84**, 1234–1242.
7 A. N. Amenaghawon, J. E. Ayere, U. O. Amune, I. C. Otuya, E. C. Abuga, C. L. Anyalewechi, O. V. Okoro, J. A. Okolie, P. K. Oyefolu, S. O. Eshiemogie, B. E. Osahon, M. Omede, S. A. Eshiemogie, S. Igemhokhai, M. O. Okedi, H. S. Kusuma, O. E. Muojama, A. Shavandi and H. Darmokoesoemo, *Environ. Res.*, 2024, **251**(Part 2), 118703.
8 T. Kayashima and T. Katayama, *Biochim. Biophys. Acta, Gen. Subj.*, 2002, **1573**, 1–3.
9 M. A. Zafar, Y. Liu and M. Jacob, *SSRN Electron. J.*, 2022, **8**, 100188.
10 Q. Zhai, *Spectrochim. Acta, Part A*, 2008, **71**(2), 332–335.
11 D. T.-S. A, K. Kawamura and L. A. Barrie, *Atmos. Environ.*, 2010, **44**, 5316–5319.
12 S. G. Yan Zhang, C. Wu and J. Zhang, *J. Electrochem. Soc.*, 2017, **164**, B29.
13 U. Nishan, A. Ahmed, N. Muhammad and M. Shah, *RSC Adv.*, 2024, **14**, 7022–7030.
14 A. Badshah, S. Noreen, M. Shah, M. Asad and R. Ullah, *RSC Adv.*, 2024, **14**, 19539–19549.
15 F. Rigoldi, S. Donini, A. Redaelli, E. Parisini and A. Gautieri, *APL Bioeng.*, 2018, **2**(1), 1–18.
16 P. Ying Gan, N. Hu, C. He, S. Zhou, J. Tu, T. Liang, Y. Pan, D. Kirsanov, A. Legin, H. Wan and P. Wang, *Biosens. Bioelectron.*, 2019, **130**, 254–261.
17 P. F. Basharzad, K. Farhadi, M. Forough and R. Molaei, *Sens. Lett.*, 2016, **14**, 906–912.
18 H. Tavallali, G. Deilamy-Rad and N. Mosallanejad, *Food Technol. Biotechnol.*, 2018, **56**, 329–336.
19 L. J. Tang and M. H. Liu, *Bull. Korean Chem. Soc.*, 2010, **31**, 3159–3162.
20 Y. Liu, J. Huang, D. Wang, H. Hou and T. You, *Anal. Methods*, 2010, **2**, 855–859.
21 N. Pourreza, N. Lotfizadeh and H. Golmohammadi, *Spectrochim. Acta, Part A*, 2018, **192**, 251–256.
22 R. N. Juine and A. Das, *ACS Sustain. Chem. Eng.*, 2020, **8**, 11579–11587.
23 L. Wu, F. Li, H. Yu, L. Shen and M. Wang, *Spectrochim. Acta, Part A*, 2023, **284**, 121784.
24 C. Cesar Souza Machado, J. F. da Silveira Petruci and S. G. Silva, *Microchem. J.*, 2021, **168**, 106466.
25 U. Nishan, I. Ullah, R. Gul, A. Badshah, N. Muhammad, N. Khan, M. Shah, M. Asad, S. Afridi, R. Ullah, E. A. Ali and S. C. Ojha, *ACS Omega*, 2023, **8**, 44931–44941.
26 U. Nishan, R. Gul, N. Muhammad, M. Asad, A. Rahim, M. Shah, J. Iqbal, J. Uddin, A. ul. H. Ali Shah and S. Shujah, *Microchem. J.*, 2020, **159**, 105382.
27 J. Singh, G. Kaur and M. Rawat, *Journal of Bioelectronics and Nanotechnology*, 2016, **1**(1), 9.
28 G. Ren, D. Hu, E. W. C. Cheng, M. A. Vargas-reus, P. Reip and R. P. Allaker, *Int. J. Antimicrob.*, 2009, **33**, 587–590.
29 N. Verma and N. Kumar, *ACS Biomater. Sci. Eng.*, 2019, **5**, 1170–1188.
30 C. K. Wu, M. Yin, S. O'Brien and J. T. Koberstein, *Chem. Mater.*, 2006, **18**, 6054–6058.
31 D. Deng, Y. Jin, Y. Cheng, T. Qi and F. Xiao, *ACS Appl. Mater. Interfaces*, 2013, **5**, 3839–3846.
32 S. Raschka, J. Patterson and C. Nolet, *Information*, 2020, **11**(4), 193.
33 F. Pedregosa, G. Varoquaux, A. Gramfort, V. Michel, B. Thirion, O. Grisel, M. Blondel, P. Prettenhofer, R. Weiss, V. Dubourg, J. Vanderplas, A. Passos, D. Cournapeau, M. Brucher, M. Perrot and É. Duchesnay, *J. Mach. Learn. Res.*, 2011, **12**, 2825–2830.
34 F. Zehra, T. Fatima and M. Khanuja, *Adv. Mater. Technol.*, 2025, **00519**, 1–18.
35 D. Renuga, J. Jeyasundari, A. S. S. Athithan and Y. B. A. Jacob, *Mater. Res. Express*, 2020, **7**, 1–7.
36 M. Bin Mobarak, M. S. Hossain, F. Chowdhury and S. Ahmed, *Arab. J. Chem.*, 2022, **15**(10), 104117.
37 U. Nishan, S. Rehman, R. Ullah, A. Bari, S. Afridi, M. Shah, J. Iqbal, H. U. Khan and N. Muhammad, *Front. Mater.*, 2023, **10**, 1–10.
38 A. S. Ethiraj and D. J. Kang, *Nanoscale Res. Lett.*, 2012, **7**, 70.
39 O. A. Bulavchenko and Z. S. Vinokurov, *Catalysts*, 2023, **13**(11), 1421.
40 G. Ravi and N. Patra, *J. Mater. Sci. Mater. Eng.*, 2025, **20**(34), 1–8.
41 W. Z. Shia, Y. S. Lianga, B. Lua, M. Chena, Y. Lia and Z. Yanga, *Quim. Nova*, 2019, **42**, 638–641.
42 M. C. Biesinger, *Surf. Interface Anal.*, 2017, **49**, 1325–1334.
43 M. Piñon-Espitia, D. Lardizabal-Gutiérrez, M. L. Camacho-Ríos, G. Herrera-Pérez and M. T. Ochoa-Lara, *Mater. Chem. Phys.*, 2021, **272**, 124981.
44 R. F. Roberts, *J. Electron Spectrosc. Relat. Phenom.*, 1974, **4**, 273–291.
45 N. Baig and T. A. Saleh, *Glob. Challenges*, 2019, **3**, 1800115.
46 X. Sun and Y. Luo, *Mater. Lett.*, 2005, **59**, 3847–3850.
47 T. Li, Y. Li, Y. Zhang, C. Dong, Z. Shen and A. Wu, *Analyst*, 2015, **140**, 1076–1081.
48 P. Aggarwal, J. S. Rana, M. Chitkara and A. Kumar, *J. Clust. Sci.*, 2024, **35**, 2093–2103.
49 W. L. Daniel, M. S. Han, J. S. Lee and C. A. Mirkin, *J. Am. Chem. Soc.*, 2009, **131**, 6362–6363.
50 F. Hong, N. O. Nilvebrant and L. J. Jönsson, *Biosens. Bioelectron.*, 2003, **18**, 1173–1181.
51 C. S. Pundir, N. Chauhan, Rajneesh, M. Verma and Ravi, *Sens. Actuators, B*, 2011, **155**, 796–803.
52 X. Chen, Z. Cai, Z. Huang, M. Oyama, Y. Jiang and X. Chan, *Nanoscale*, 2013, **5**, 5779–5783.